Catena 127 (2015) 177–190

Contents lists available at ScienceDirect

Catena

journal homepage: www.elsevier.com/locate/catena

Sediment and nutrient dynamics during storm events in the Enxoé temporary river, southern Portugal

Tiago B. Ramos [a], Maria C. Gonçalves [b,*], Maria A. Branco [b], David Brito [a], Sara Rodrigues [b], José-Miguel Sánchez-Pérez [c,d], Sabine Sauvage [c,d], Ângela Prazeres [b], José C. Martins [b], Manuel L. Fernandes [b], Fernando P. Pires [b]

[a] MARETEC, Instituto Superior Técnico, Universidade de Lisboa, Lisbon, Portugal
[b] INIAV, Instituto Nacional de Investigação Agrária e Veterinária, Oeiras, Portugal
[c] Université de Toulouse, INPT, UPS, Laboratoire Ecologie Fonctionelle et Environnement (ECOLAB), Ecole Nationale Supérieure Agronomique de Toulouse (ENSAT), Castanet Tolosan, France
[d] CNRS, Laboratoire Ecologie Fonctionnelle (ECOLAB), Castanet Tolosan, France

ARTICLE INFO

Article history:
Received 7 April 2014
Received in revised form 28 December 2014
Accepted 2 January 2015
Available online xxxx

Keywords:
Storm events
Hysteresis
Nitrate
Phosphorus
Suspended sediments

ABSTRACT

In temporary (or intermittent) rivers the first storm event after a dry period is responsible for transferring large amounts of sediment and nutrients into water reservoirs, thereby justifying close monitoring. The objective of this study was to analyse the contribution of storm events to sediment and nutrient transport in the Enxoé temporary river (southern Portugal) using detailed monitoring collected during three hydrological years (September, 2010 to August, 2013), and identify possible sediment and nutrient source areas based on the interpretation of hysteresis in the concentration–discharge relationship. The Enxoé River was monitored for suspended sediment concentration (SSC), total phosphorus (TP), particulate phosphorus (PP), soluble reactive phosphorus (SRP), and nitrate (NO_3^-). An empirical model was used to describe changes in solute concentrations, and the magnitude and rotational patterns of the hysteretic loops. Twenty-one storm events were registered. SSC, TP, PP, SRP, and NO_3^- concentrations varied between 1.6 and 3790.1, 0.05–11.4, 0–7.6, 0–0.67, and 0–27.84 mg l^{-1}, respectively. The highest SSC, TP, and PP concentrations were registered during the first storm event after an extended drought period. Annual sediment yields (13–480 kg ha^{-1} y^{-1}) and nitrate (4.4–45.5 kg ha^{-1} y^{-1}) were relatively low, while phosphorus losses (0.04–0.96 kg ha^{-1} y^{-1}) reached relatively high values during humid years. Sediment and phosphorus transport was influenced by the stream transport capacity and particle availability, whereas nitrate loads were influenced by rainfall, soil hydraulic characteristics, and land management. This work highlights the main processes involved in sediment and nutrients loads in a temporary river during storm events, with a quantification of the relevant elements.

1. Introduction

Suspended sediment transport from agricultural catchments to stream networks is responsible for aquatic habitat degradation, reservoir sedimentation and the transport of sediment-bound pollutants (pesticides, particulate, nutrients, heavy metals and other toxic substances). Storm events are a natural phenomenon responsible for increasing the transport of sediments and nutrients into streams and lakes. Such events can result in pollution peaks that can last from a few minutes to a few days, leading to the eutrophication of water bodies, and to the contamination of drinking water and ecosystems (Langlois et al., 2005; Yevenes and Mannaerts, 2011). In the particular case of southern European regions, storm events appear to contribute substantially to phosphorus and nitrogen removal due to the characteristics of the Mediterranean climate and soils, as well as land use (Torrent et al., 2007). Phosphorus, which is usually considered the limiting nutrient to primary production, is mainly transferred from agricultural soils through runoff and soil erosion, as inorganic P forms bound preferentially to soil sediments through interactions with iron or aluminium oxy-hydroxides (Skoulikidis and Amaxidis, 2009; Oeurng et al., 2010a; Zhu et al., 2012). Nitrogen, which may also play an important role in autotrophic production, namely in the nitrate form, is more often transported through subsurface flow (Sánchez-Pérez et al., 2003; Buda and DeWalle, 2009; Oeurng et al., 2010b; Cerro et al., 2013).

However, finding a direct relationship between water quality deterioration and storm events characteristics is not straightforward as it depends on the catchment topography, hydro-morphology, land use and management, and the remobilisation of sediments and pollutants (Klein and Koelmans, 2011; Zhu et al., 2012). These complex relationships are even more undetermined in catchments with intermittent

* Corresponding author at: Instituto Nacional de Investigação Agrária e Veterinária, Quinta do Marquês, Av. República, 2784-505 Oeiras, Portugal.
E-mail address: maria.goncalves@iniav.pt (M.C. Gonçalves).

http://dx.doi.org/10.1016/j.catena.2015.01.001
0341-8162/

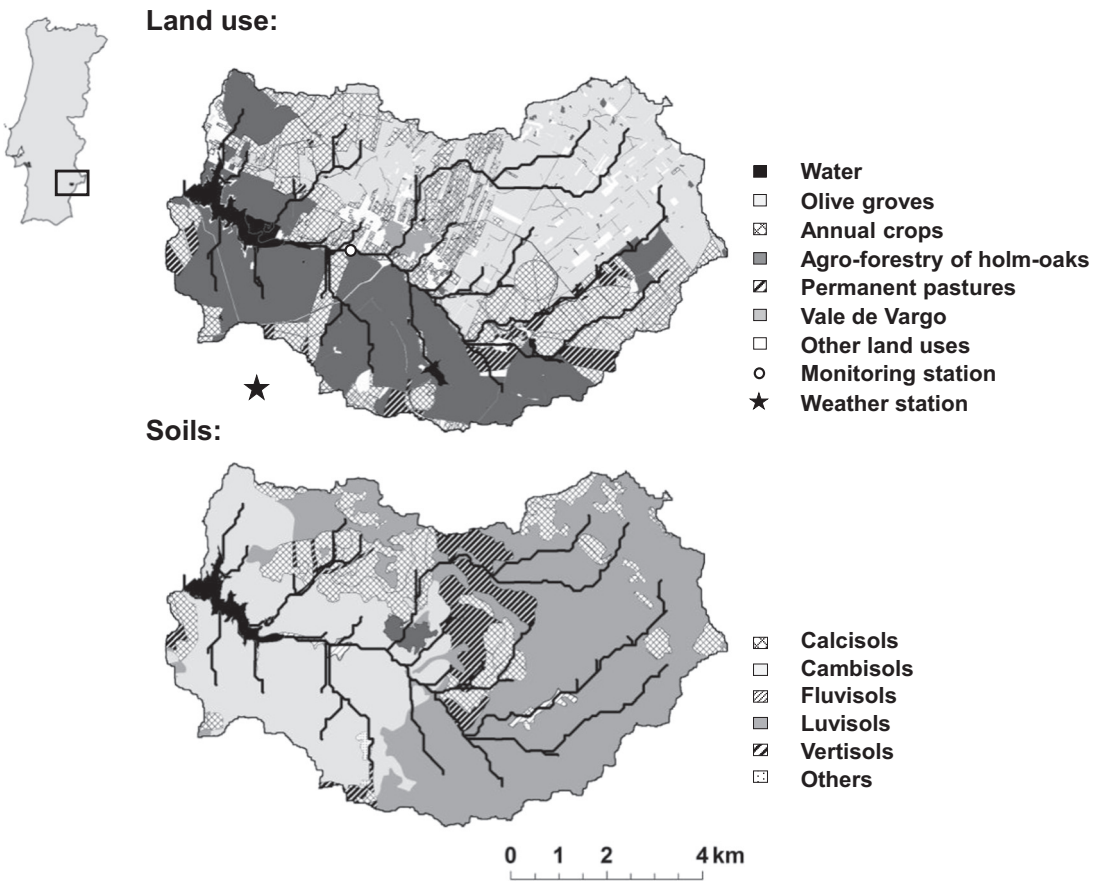

Fig. 1. Location of the Enxoé catchment in Portugal. Land use (top) and major soil units (bottom) in the Enxoé catchment.

(herein termed temporary) rivers located in semi-arid regions where those phenomena remain largely unassessed (Alexandrov et al., 2003; Rovira and Batalla, 2006; Torrent et al., 2007; Butturini et al., 2008). In these water scarce regions studies with a high sampling density as the one presented here, focusing on the hydrological and biogeochemical regimes of temporary rivers are very rare, but are crucial for implementing effective conservation measures and other good agricultural practices.

These temporary streams, over an annual cycle, form small lentic shallow systems where sediments and nutrients accumulate, and lotic systems where high flushing rates are often registered. During dry periods with flow cessation followed by pool formation, the shallowness of the water column associated with the low discharge and high temperatures may enhance important biochemical processes at the sediment/water column interface leading to the accumulation of nutrients. During storm events, surface or subsurface flow becomes more enriched with sediment and dissolved nutrients accumulated in those pools with severe implications for the physical and chemical environment of the water bodies (Lillebø et al., 2007). However, sediment and nutrient dynamics in temporary rivers may also be related to rainfall–runoff processes and to the type of storm. High-intensity, convective or convective-enhanced storms during autumn and spring have already been associated with higher sediment yields, while lower-intense, long-duration, frontal storms occurring during winter have been related to lower sediment yields (Alexandrov et al., 2007). Hence, sediment and nutrient dynamics in these temporary streams is mainly determined by seasonality and sequences of dry periods and the following storm events (Lillebø et al., 2007; Alexandrov et al., 2007), providing a difficult challenge in developing sustainable water management plans (Tzoraki and Nikolaidis, 2007).

Monitoring programmes are thus essential for understanding the hydrological regime of a temporary river, sediment and nutrient dynamics across the catchment, and the effect of storm events on basic functions of ecosystems, namely, on soil retention, and water and nutrient regulation. Long-term nutrient concentrations datasets are important to understand nutrient trends, loads, nutrient behaviour, the effectiveness of past nutrient migration, and supporting data for future management decisions regarding issues of eutrophication and nutrient control (Burt, 2003; Oeurng et al., 2010b). Nevertheless, while monitoring of nutrient concentration is important in determining the nutrient status of a water body, it does not necessarily provide information on the source of those sediments and nutrients. That information may be obtained by analysing the hysteresis in the concentration–discharge relationship (House and Warwick, 1998; Bowes et al., 2005; Eder et al., 2010; Oeurng et al., 2010a). Hysteresis, at a given discharge, is characterised by differences in the concentration of an element on the rising and falling limb of a hydrograph. When plotted, that relationship may show clockwise or anticlockwise loop trajectories that give an insight on the source of the eroded materials. Other methods, likely more precise, include the development of modelling tools for mapping soil erosion (Oeurng et al., 2011; Borrelli et al., 2014), the use of rare earth elements as tracers (Stevens and Quinton, 2008), and fingerprinting (Martínez-Carreras et al., 2010; Siebert et al., 2014). This latter approach relies on the identification of physical, geochemical, mineralogical, and mineral magnetic properties, which clearly differentiate potential source materials. These properties are then compared with measurements of the same property obtained from suspended sediment in order to identify the likely source of that material (Walling, 2005). Additionally, isotopic signatures and the activity of fallout radionuclides may also be applied to complement fingerprinting, allowing to distinguish between surface and subsurface materials, cultivated and uncultivated soils, and even soil types (Motha et al., 2003; Wallbrink et al., 2003; Walling, 2005).

Table 1
Summary description of the main agricultural practices carried out in the Enxoé catchment area.

Land use	Tillage operations	Fertilisation inputs[a]	Livestock
Olive groves	Traditional olive groves (<100 trees ha^{-1}):	Traditional olive groves (<100 trees ha^{-1}):	Sheep (0.1 LSU[b])
	Harrowing (October)	24 kg ha^{-1} of N (April and May)	
	Intensive olive groves (300–500 trees ha^{-1}):	Intensive olive groves (300–500 trees ha^{-1}):	
	No tillage; average irrigation depths 200 mm/year (MADRP, 2010)	60 kg ha^{-1} of N (April to July) 15 kg ha^{-1} of P (April to July) 30 kg ha^{-1} of K (April to July)	
Agro-forestry of holm-oaks	Areas with >30 trees ha^{-1}: Harrowing (May) Areas with <30 trees ha^{-1}: Include also annual winter crops Harrowing (October)	Annual winter crops: Triticale and Oats 40–80 kg ha^{-1} of N (October to November) 60 kg ha^{-1} of P (October to November)	Cows, sheep, goats, and pigs (0.4 LSU, which increase to 0.6 LSU for 3 months during holm-oaks fructification period)
Annual winter crops: Rotation 1 (sunflower + wheat or triticale + barley or oats)	Sunflower: Moldboard ploughing (April) Harrowing (April) Heavy rolling (April) Sowing (April) Harvest (September)	Sunflower: 22 kg ha^{-1} of P (April) 42 kg ha^{-1} of K (April) Wheat, Triticale and Barley: 20 kg ha^{-1} of N (November) 18 kg ha^{-1} of P (November)	Cows and sheep (0.6 LSU)
Rotation 2 (wheat or triticale + oats + fallow)	Wheat, Triticale and Barley:	50–90 kg ha^{-1} of N (January to February)	
Rotation 3 (oats + fallow)	Harrowing (November) Sowing (November) Harvest (June) Oats: Harrowing (November) Sowing (October) Harvest (June)	Oats: 40 kg ha^{-1} of N (March)	
Permanent pastures	No tillage operations	18 kg ha^{-1} of P (October)	Cows and sheep (0.6 LSU)

[a] Values obtained by questioning the farmers in the region.
[b] LSU — livestock units.

This study analyses the temporal variability of suspended sediment concentration (SSC), phosphorus (in both soluble and particulate forms), and nitrate (NO_3^-) in the Enxoé temporary river, southern Portugal, during three years of intense hydro-biogeochemical monitoring. This river was selected as the Enxoé reservoir exhibits the highest eutrophic state in Portugal, and is located in a region where many others are also classified as eutrophic (CCDR Alentejo, 2005; Instituto da Água, 2008). The study focuses on solids and solutes transport in this temporary Mediterranean river, with special emphasis on their pattern during storm episodes (i.e., concentration–discharge relationships). The analysis of concentration–discharge responses in Mediterranean streams is still in a preliminary phase, and even rarer are those studies that explored these responses in Mediterranean human-altered systems, like Enxoé.

This study focuses on the contribution of storm events to sediment and nutrient transport in the Enxoé temporary river using detailed monitoring carried out during three hydrological years (September, 2010 to August, 2013). It also highlights the importance of monitoring the first storm events after a dry period. Finally, the possible sediment and nutrient source areas and associated processes are also identified based on the interpretation of hysteresis in the concentration–discharge relationship. The data presented here are relatively rare in the case of temporary rivers, and may help decision-makers to improve the management of drinking water catchment areas by minimising pollution risks during storm events and reducing the trophic state of freshwater reservoirs.

2. Material and methods

2.1. Catchment description

The Enxoé catchment is located in the Alentejo region, southern Portugal (Fig. 1). The river is a tributary of the Guadiana river, has a bed length of 9 km, a catchment area of 6080 ha, and an altitude ranging from 155 to 348 m.

The dominant soils are Luvisols (covering 47% of the area), Cambisols (31%), and Calcisols (14%). The main magmatic and sedimentary rocks include granites, schists, greywackes, limestone, diorites, and quartzodiorites. The main land uses are olive groves (1830 ha), agro-forestry of holm-oaks (1760 ha), and annual winter crops (1700 ha). The main agricultural practices are summarised in Table 1. Average fertilisation inputs are estimated to amount 25 kg N ha^{-1} y^{-1} and 12 kg P ha^{-1} y^{-1}, while animal excretions are estimated to reach 26 kg N ha^{-1} y^{-1} and 3 kg P ha^{-1} y^{-1} (Table 1; Agroscope, 2009). Hence, nutrient inputs in the Enxoé catchment can be considered low when compared with more intensive agricultural catchments (e.g., Yevenes and Mannaerts, 2011).

The climate is dry sub-humid to semi-arid. The precipitation regime is characterised by a highly irregular behaviour, varying between relatively abundant rainfall episodes, concentrated in only a few minutes or hours, and frequent drought episodes that can last from a few months to a couple of years. The annual average precipitation is 500 mm, irregularly distributed throughout the year (80% of the annual precipitation is concentrated between October and April). Thus, the hydrological regime causes a strong inter and intra-annual variation of the discharges. From fall to spring, the river frequently presents high flow discharges after storm events. During summer, the river normally exhibits no flow. As a result, the hydrological year is defined between September and August of the following calendar year. The annual average temperature is 16 °C, and the annual reference evapotranspiration varies between 1200 and 1300 mm. Weather data used in this study was collected from a weather station located in Herdade da Valada, Serpa (Fig. 1).

The catchment has a population of 1000 inhabitants, mainly concentrated in Vale de Vargo (Fig. 1), and is limited downstream by a dam (10.4 million m^3) built in 2000, which supplies the villages of Mértola

and Serpa (25,000 inhabitants). There are no point source emissions in Enxoé. The waste waters of the treatment plant of Vale de Vargo are pumped to a water stream located outside the Enxoé catchment area.

2.2. River Enxoé water quality monitoring

The river Enxoé water was monitored at the sampling station located upstream the reservoir (Fig. 1) during three hydrological years (September, 2010 to August, 2013). The upstream drainage area covers approximately 2/3 of the watershed (45 km^2). Sampling waters was undertaken for suspended sediment concentration (SSC), total phosphorus (TP), particulate phosphorus (PP) consisting of phosphorus adsorbed to particulate suspended material (>0.45 μm), soluble reactive phosphorus (SRP), and nitrate (NO_3^-). An YSI 6920 measuring probe (YSI Incorporated, Ohio, USA) was used to monitor the water stream level and turbidity (by nephelometry) continuously. Readings were taken every 15 min during storm events and daily during non-storm events. Flow was then obtained from the measured water level with the well-established Gauckler–Manning formula. Manning's roughness coefficient was set to 0.06. Variations in vegetative roughness were not accounted for, thus leading to some uncertainty when estimating flow throughout different seasons. An automatic water sampler (EcoTech Umwelt-Meβsysteme GmbH. Bonn, Germany) with 8 bottles, 2 l each, was used for monitoring water quality during storms. The monitoring station was positioned near the bank of the river, where the movement of water was considered representative of river flow. The pump inlet of the automatic water sampler was placed next to the measuring probe pipe. The probe was programmed to activate the automatic water sampler when the water level varied more than 10 cm on both rising and falling stages of storm events. As a result, automatic sampling varied from 3 min (during flash events) to 15 h during storm events. Manual sampling was also carried out at weekly intervals using 2 l bottles collected near the probe location. The total number of water samples taken from both automatic and manual sampling was 176.

Water samples (250–1000 ml) were filtered in the laboratory to determine SSC using pre-weighed glass microfiber paper (GFF 0.75 μm). The sediments retained on the filter paper were oven dried at 50 °C over 24 h. The filters were again weighed and SSC was calculated.

Aliquots of each sample were filtered using a cellulose acetate membrane (0.45 μm), and analysed for total dissolved phosphorus (TDP), SRP, and NO_3^-. TP was determined in the unfiltered samples. TP and TDP were quantified, after sulphuric acid and nitric acid digestion, colourimetrically by reacting with ammonium molybdate. SRP was also quantified colourimetrically, using the same reaction (APHA, 1995). PP was determined from the difference between TP and TDP concentrations. NO_3^- concentration was measured directly in the filtered solution with an automated segmented flow analyser, using the cadmium reduction method (Hendrilsen and Selmer-Olsen, 1970).

2.3. Water, sediment, and nutrient loads

Water yield was determined by integrating river discharge over a time period (3 to 15 min during storm events and daily during non-storm events), as follows:

$$W = \sum_i \frac{\left(Q_{(i)} + Q_{(i-1)}\right)}{2} \times \left(t_{(i)} - t_{(i-1)}\right) \quad (1)$$

where W is the accumulated water yield (l^3), and Q_i is the instantaneous river discharge ($l^3\ T^{-1}$) at time i (T).

Sediments and nutrient loads were obtained by averaging concentrations between two adjacent samples and integrating this with discharge. Continuous sediment and nutrient series were thus developed to reduce uncertainty that would result from interpolation and extrapolation of low-frequency measurements. The continuous data series for the particulate elements were based on the SSC-turbidity, TP-turbidity, and PP-turbidity relations found in Enxoé, and were only possible due to the quasi-continuous turbidity recording provided by the automatic probe (15 min during storm events and daily during non-storm events) which complemented the information collected with the automatic water sampler (3 min to 15 h during storm events). The relationships between turbidity readings and SSC, TP, and PP

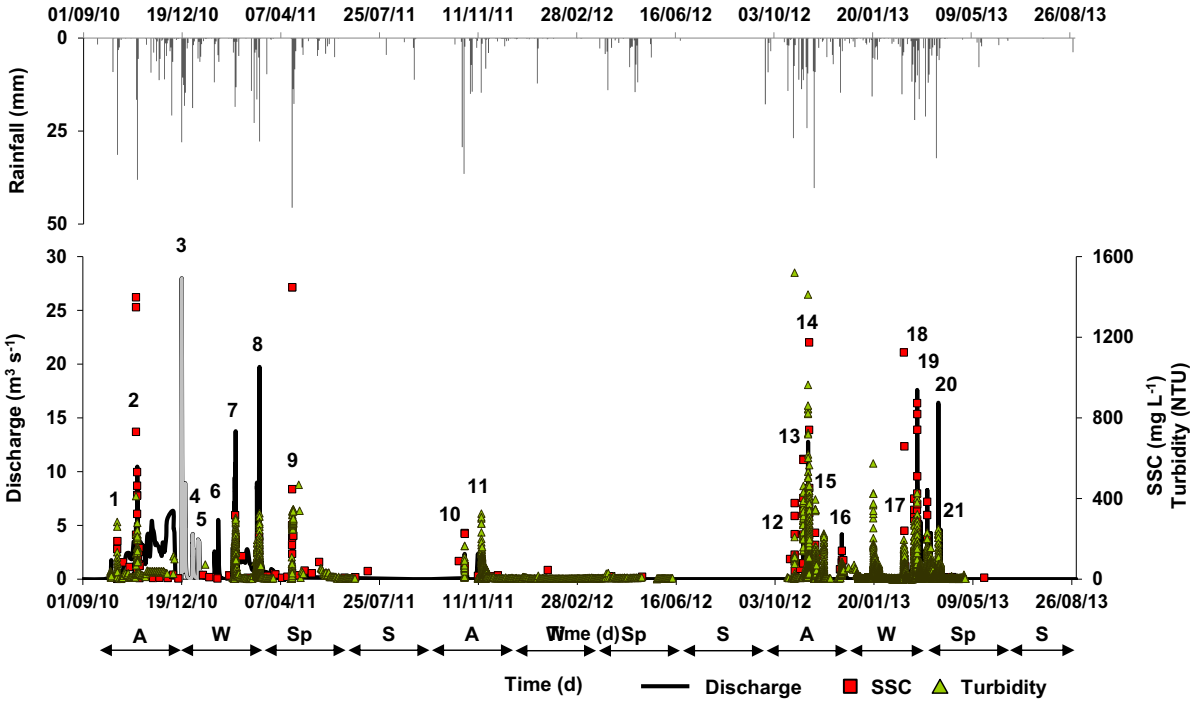

Fig. 2. Rainfall, Discharge, suspended solid concentration (SSC), and turbidity monitored between September, 2010 and August, 2013. The line in light grey represents the period of 22 days when the equipment malfunctioned. A, W, Sp, and S correspond to autumn, winter, spring, and summer, respectively.

Table 2
General characteristics of the storm events observed in the Enxoé catchment between September, 2010 and August, 2013.[a]

Storm events		Rainfall							Discharge			
No.	Date	FD	W	Pe	Pd	P1	P5	P10	Q_{mean}	Peak	Q_{max}	T_{peak}
		(h)	($\times 10^6$ m^3)	(mm)	(h)	(mm)	(mm)	(mm)	(m^3 s^{-1})	N°	(m^3 s^{-1})	(h)
Year 1 (Sept. 2010 to Aug. 2011)												
1	08/10–11/10	52	0.05	37	4	31	32	41	1.3	1st	3.6	1.0
2	29/10–02/11	48	0.51	60	3	17	17	17	5.2	1st	5.2	0.5
										2nd	10.5	34.4
										3rd	8.2	38.6
3	18/12–23/12	127	0.62	84	4	11	39	40	5.4	1st	28.0	9.0
										2nd	8.7	66.4
										3rd	8.9	98.7
4	30/12–02/01	92	0.50	22	3	19	19	56	1.5	1st	4.2	25.2
5	07/01–09/01	70	0.27	13	2	6	13	35	1.0	1st	3.5	4.0
6	28/01–31/01	63	0.33	7	4	6	14	26	1.5	1st	5.5	4.0
7	15/02–17/02	69	1.31	33	7	19	24	24	4.8	1st	7.2	3.5
										2nd	9.5	9.2
										3rd	13.8	33.7
8	14/03–15/03	43	0.94	28	3	28	53	94	5.9	1st	10.6	6.8
										2nd	19.7	18.9
9	19/04–21/04	40	0.16	77	7	46	46	46	0.9	1st	6.2	8.5
Year 2 (Sept. 2011 to Aug. 2012)												
10	26/10–28/10	29	0.07	68	4	37	67	67	0.6	1st	2.4	2.0
11	09/11–10/11	36	0.15	37	4	14	37	76	0.1	1st	2.4	4.0
Year 3 (Sept. 2012 to Aug. 2013)												
12	24/10–24/10	2	0.01	27	1	27	28	46	1.4	1st	3.0	0.5
13	03/11–05/11	4	0.05	20	5	8	33	43	3.0	1st	4.3	2.0
14	08/11–10/11	41	0.43	34	3	24	43	77	2.7	1st	12.8	4.5
										2nd	4.9	36.8
15	16/11–17/11	33	0.14	49	2	40	49	91	1.2	1st	3.1	2.3
										2nd	2.7	21.0
16	15/12–17/12	57	0.26	15	5	15	17	29	1.2	1st	4.2	10.3
										2nd	2.5	54.8
17	19/01–20/01	21	0.11	21	1	16	17	21	1.5	1st	3.7	2.8
18	04/03–14/03	234	1.42	85	2	7	20	21	2.6	1st	6.4	9.0
										2nd	5.9	59.4
										3rd	17.6	88.0
										4th	5.3	177.7
19	19/03–21/03	29	0.35	21	3	21	24	53	3.3	1st	8.3	5.8
20	23/03–25/03	43	0.43	13	2	10	43	46	2.7	1st	4.3	2.5
21	31/03–05/04	100	1.18	46	5	32	37	66	3.6	1st	16.4	11.3
										2nd	4.6	71.3

[a] FD, flow duration; W, water yield; Pe, total amount of rainfall registered between the rising and recession limbs of the same storm event; Pd, rainfall duration during a storm event; P1, P5, and P10, cumulative precipitation one, five and ten days before the first discharge peak, respectively; Q_{mean}, mean discharge; Q_{max}, discharge peak; T_{peak}, time of rise.

concentrations were obtained by linear regression. This approach is commonly found in the literature (e.g., Langlois et al., 2005; Lefrançois et al., 2007; López-Tarazón et al., 2009; Eder et al., 2010; Oeurng et al., 2010a; Cerro et al., 2013). The solute elements (SRP and NO_3^-) were estimated from the high frequency of data collection provided by the automatic sampler (3 min to 15 h during storm events and weekly during non-storm events). Sediments and nutrient loads were thus linear interpolated between two adjacent samples, as follows:

$$M_d = \sum_i \frac{\left(C_{d(i)} + C_{d(i-1)}\right)}{2} \times W_i \quad (2)$$

where M_d is the solute mass lost in the catchment from diffuse (d) sources (M), and C_i and W_i are the instantaneous solute concentration (M^{-3}) and water yield (l^3), respectively, at time i (T).

2.4. Solute-discharge hysteresis analysis

For each storm event, the analysis of the concentrations (C) of SSC, TP, PP, SRP, and NO_3^- versus discharge (Q) relationships, was performed with the approach proposed by Butturini et al. (2006). The shape, rotational patterns and trends of hysteretic loops of each determinand are described here with two parameters: the changes in solute concentrations (ΔC), and the overall dynamics of each hysteretic loop (ΔR).

ΔC (%) describes the relative changes in solute concentration and hysteresis trend, as follows:

$$\Delta C = (C_s - C_b)/C_{max}\,100 \quad (3)$$

where C_b and C_s are the solute concentrations at base flow and at peak discharge, respectively, and C_{max} is the highest concentration observed in the stream during a storm. ΔC ranges from −100 to 100%, where positive values indicate solute flushing, and negative values solute dilution. For solute flushing, maximum ΔC (100%) is obtained when $C_s = C_{max}$ and $C_b = 0$. For solute dilution, minimum ΔC (−100%) is obtained when $C_s = 0$ and $C_b = C_{max}$. All other situations where the concentration peak (C_{max}) arrives before or after the peak discharge (C_s) fall within that interval.

The ΔR (%) descriptor integrates information about the magnitude (area) and direction (rotational pattern) of the C–Q hysteresis, as follows:

$$\Delta R = R\ A_h\ 100 \quad (4)$$

where A_h is the area of the C–Q hysteresis loop, estimated after standardising discharges and concentrations to a unity scale, which

means that A_h will be lower than unity. If A_h is closer to zero, the relationship pattern is more linear shaped, i.e., the concentration in the rising limb is similar to the concentration in the recession limb for the same discharge. If A_h is closer to unity, the area of the hysteresis loop is larger, and the concentration of the rising limb is different from the concentration in the recession limb for the same discharge. R summarises the rotational pattern of the C–Q hysteresis. If the C–Q hysteresis is clockwise, then $R = 1$; if anticlockwise, then $R = -1$; for unclear (for example, figure-of-eight-shaped hysteresis loops) or non-existent hysteresis, $R = 0$. ΔR thus ranges also from −100 to 100%.

The variability of the C–Q hysteresis descriptors for the different determinands is described in a plot of ΔC vs ΔR, where four regions can be identified according to flushing/dilution of the constituent and the hysteresis loop sense (clockwise or anticlockwise). All this information allows clarification of the source of particulate matter and soluble elements, and separation of different types of storms. Further details can be found in Butturini et al. (2006, 2008).

3. Results

3.1. General description of monitored storm events

Twenty-one storm events occurred between September, 2010 and August, 2013 (Fig. 2). These events took place during autumn (10), winter (8), and spring (3). During summer there was no flow in the river.

Total precipitation amounted to 695, 270, and 570 mm during the first (2010/2011), second (2011/2012), and third (2012/2013) hydrological years, respectively. The first year can thus be classified as humid, the second as very dry, and the third as within the average (≈500 mm). River discharge reflected those rainfall amounts, with annual water yielding 28.7×10^6, 1.3×10^6, and 10.1×10^6 m^3 in 2010/2011, 2011/2012, and 2012/2013, respectively. Major rainfall events generally occurred in autumn (October/December) and spring (March/April). Storm events lasted between 1.8 and 233.5 h (mean = 58.7 h; standard deviation, $\sigma = 50.1$ h). Seven events lasted longer than the average duration. Maximum discharge varied between 2.4 and 28.0 $m^3 s^{-1}$ (mean = 7.6 $m^3 s^{-1}$; $\sigma = 5.7$ $m^3 s^{-1}$). Nine events produced multiple discharge peaks. The mean rising time to reach the first discharge peak was 5.7 h ($\sigma = 5.5$ h). The shortest time was only 0.5 h. Water yield ranged from 0.01×10^6 to 1.42×10^6 m^3 (mean = 0.44×10^6 m^3; $\sigma = 0.43 \times 10^6$ m^3). Seven events produced higher water yields than average. Table 2 summarises the main characteristics of all registered storm events.

Flow duration (FD) was positively correlated at $P < 0.001$ level to water yield (W), and to the number of peak discharges registered during a storm event (Pk_n); and at $P < 0.01$ level to maximum discharge (Q_{max}) (Table 3). W was positively correlated at $P < 0.001$ level to Pk_n; and at $P < 0.01$ level to Q_{max} and mean discharge (Q_{mean}). Q_{max} was also correlated at $P < 0.001$ level to Pk_n, Q_{mean}, and to the first peak discharge ($Q_{peak\ 1}$). Finally, Q_{mean} was further correlated at $P < 0.01$ level to Pk_n and $Q_{peak\ 1}$.

3.2. Temporal variation of suspended sediments, phosphorus forms and nitrate concentrations

The relations found between turbidity readings taken with the automatic probe and SSC, TP, and PP concentrations measured in the river (Fig. 2 and 3) were the following:

$$\mathrm{SSC}\left(\mathrm{mg\,l^{-1}}\right) = 2.493\ \mathrm{turbidity\ (NTU)} \quad \left(R^2 = 0.86,\ n = 99\right) \tag{5}$$

$$\mathrm{TP}\left(\mathrm{mg\,l^{-1}}\right) = 0.010\ \mathrm{turbidity\ (NTU)} \quad \left(R^2 = 0.80,\ n = 70\right) \tag{6}$$

$$\mathrm{PP}\left(\mathrm{mg\,l^{-1}}\right) = 0.008\ \mathrm{turbidity\ (NTU)} \quad \left(R^2 = 0.80,\ n = 92\right). \tag{7}$$

These linear regressions were used to derive SSC, TP, and PP from turbidity, thus complementing direct measurements of these elements taken with the automatic sampler. They confirmed the close relationship between turbidity, SSC, TP, and PP, and that the quasi-continuous turbidity measurements could be used to more accurately estimate the loads of the particulate elements and analyse their hysteresis patterns. The following relationships between SSC, TP, and PP were also found:

$$\mathrm{TP}\left(\mathrm{mg\,l^{-1}}\right) = 0.003\ \mathrm{SSC}\left(\mathrm{mg\,l^{-1}}\right) \quad \left(R^2 = 0.85,\ n = 80\right) \tag{8}$$

$$\mathrm{PP}\left(\mathrm{mg\,l^{-1}}\right) = 0.002\ \mathrm{SSC}\left(\mathrm{mg\,l^{-1}}\right) \quad \left(R^2 = 0.82,\ n = 124\right) \tag{9}$$

which may show to be useful in future studies carried out in the Enxoé catchment.

SSC was at a minimum (2.0–215.0 mg l^{-1}) during non-storm events and at a maximum (1.6–3790.1 mg l^{-1}) during storm events (Fig. 2). The maximum measured value (1447.9 mg l^{-1}) was reached in April, 2011 (event 9). However, the maximum turbidity value (1520.3 NTU = 3790.1 mg l^{-1}) was observed in October, 2012, during the first flood

Table 3
Pearson correlation matrix between sediment and nutrient yields and the hydro-climatological variables[a,b] (n = 21 storm events).

	S	FD	W	Pe	Pd	P1	P5	P10	Q_{mean}	Pk_n	$Q_{peak\ 1}$	Q_{max}	T_{peak}	SS	TP	NO_3
S	1.00															
FD	−0.23	1.00														
W	−0.41	***0.73***	1.00													
Pe	0.09	0.50	0.28	1.00												
Pd	−0.18	−0.01	0.22	0.17	1.00											
P1	−0.05	−0.32	−0.18	0.35	0.25	1.00										
P5	0.06	−0.25	−0.12	0.38	0.16	***0.64***	1.00									
P10	0.09	−0.28	−0.10	0.02	−0.06	***0.55***	***0.74***	1.00								
Q_{mean}	−0.10	0.22	***0.63***	0.18	0.14	−0.17	0.02	−0.05	1.00							
Pk_n	0.10	***0.70***	***0.76***	***0.57***	0.09	−0.18	−0.12	−0.22	***0.61***	1.00						
$Q_{peak\ 1}$	0.12	0.32	0.29	0.38	0.07	−0.16	0.14	0.02	***0.61***	0.45	1.00					
Q_{max}	0.04	***0.53***	***0.61***	0.47	0.07	−0.21	0.07	−0.05	***0.77***	***0.73***	***0.87***	1.00				
T_{peak}	−0.32	0.46	0.33	0.05	0.18	−0.03	−0.17	0.09	0.09	0.08	0.16	0.14	1.00			
SS	−0.02	***0.66***	***0.75***	0.51	0.04	−0.16	0.02	−0.07	***0.62***	***0.85***	***0.60***	***0.82***	0.13	1.00		
TP	−0.04	0.46	***0.66***	0.43	0.10	−0.08	0.11	0.04	***0.71***	***0.76***	***0.72***	***0.84***	0.10	***0.95***	1.00	
NO_3	−0.06	0.26	0.29	***0.53***	0.32	−0.08	−0.14	−0.41	0.45	0.51	0.47	0.50	0.10	0.38	0.40	1.00

[a] S, season; FD, flow duration; W, water yield; Pe, total amount of rainfall registered between the rising and recession limbs of the same storm event; Pd, rainfall duration during a storm event; P1, P5, and P10, cumulative precipitation one, five and ten days before the first discharge peak, respectively; Q_{mean}, mean discharge; Pk_n, number of peak discharges; Q_{max}, maximum discharge peak; T_{peak}, time of rise; SS, suspended sediment yields; TP, total phosphorus yields; NO_3, nitrate yields.
[b] Correlation is significant at $P < 0.001$ level for underlined bold italic numbers, at $P < 0.01$ for bold italic numbers, and at $P < 0.05$ for italic numbers.

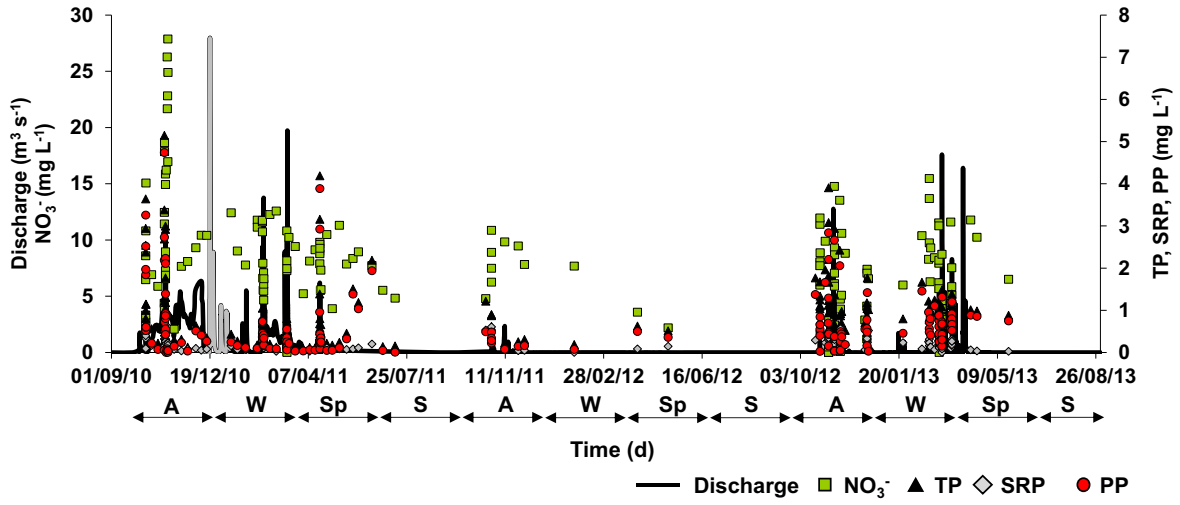

Fig. 3. Discharge, nitrate (NO_3^-), total (TP), particulate (PP) and soluble reactive (SRP) phosphorus concentrations observed between September, 2010 and August, 2013. The line in light grey represents the period of 22 days when the equipment malfunctioned. A, W, Sp, and S correspond to autumn, winter, spring, and summer, respectively.

event of 2012/2013 (event 12). Higher suspended sediment concentration generally coincided with higher rainfall intensities.

P concentrations varied between storm events and seasons (Fig. 3). Maximum values were again observed during storm events. TP values ranged from 0.05 to 11.4 mg l^{-1}. PP varied from 0 to 7.6 mg l^{-1}. TDP varied between 0.01 and 1.34 mg l^{-1}. SRP ranged from 0 to 0.67 mg l^{-1}. Maximum measured values were obtained in October, 2010 (event 2), when SSC also reached a high value. Maximum P values estimated from turbidity readings were obtained in October, 2012 (event 12). PP and TDP fractions averaged 56.3 and 44.5% of TP during most events, respectively. SRP contribution to TDP varied between 49% and 97%. SRP constituted only a small fraction of TP, but reached values of >35% in 6 events. Nitrate (NO_3^-) varied between 0 and 27.8 mg l^{-1}. The maximum value observed was reached also during event 2.

3.3. Suspended sediments, total phosphorus and nitrate loads assessment

During storm events, sediment transport ranged from 1×10^3 to 543×10^3 kg (Table 4), and was higher during autumn and early spring (end of February and March; defined based on Tables 5 and 6) (Fig. 4). Maximum load was obtained in March, 2013 (event 18), which also corresponded to the event with maximum water yield (1.42×10^6 m^3).

Table 4
Water yield and sediment and nutrient loads at the outlet between September, 2010 and August, 2013.

Storm event	Water yield		Sediment		TP		NO_3^-	
	($\times 10^6$ m^3)	(%)	($\times 10^3$ kg)	(%)	(kg)	(%)	($\times 10^3$ kg)	(%)
Year 1 (Sept. 2010 to Aug. 2011)								
1	0.05	0.2	25	1.2	76	1.8	0.3	0.1
2	0.51	1.8	205	9.5	616	14.3	10.2	5.0
3	0.62	2.2	367	17.0	1094	25.4	9.9	4.8
4	0.50	1.7	29	1.4	91	2.1	2.8	1.4
5	0.27	0.9	10	0.5	24	0.6	1.1	0.5
6	0.33	1.2	13	0.6	38	0.9	0.3	0.1
7	1.3	4.6	318	14.7	812	18.9	7.4	3.6
8	0.94	3.3	256	11.8	758	17.6	0.6	0.3
9	0.16	0.6	72	3.3	216	5.0	7.5	3.7
Total (storm events)	4.68	16.3	1296	60.0	3726	86.5	40.1	19.6
Total (year)	28.74	–	2161	–	4308	–	204.8	–
Year 2 (Sept. 2011 to Aug. 2012)								
10	0.07	5.4	1	2.7	4	2.5	0.0	0.2
11	0.15	12.0	2	3.2	5	2.7	3.3	16.7
Total (storm events)	0.22	17.5	3	5.9	9	5.2	3.3	16.9
Total (year)	1.27	–	56	–	168	–	19.7	–
Year 3 (Sept. 2012 to Aug. 2013)								
12	0.01	0.1	6	0.3	17	0.4	0.3	0.5
13	0.05	0.5	34	2.0	102	2.7	0.0	0.1
14	0.43	4.3	459	27.6	1356	35.8	0.7	1.0
15	0.14	1.4	28	1.7	83	2.2	0.5	0.7
16	0.26	2.6	35	2.1	106	2.8	1.5	2.2
17	0.11	1.1	41	2.5	123	3.3	3.0	4.4
18	1.42	14.0	543	32.7	860	22.7	2.6	3.9
19	0.35	3.4	62	3.7	185	4.9	0.6	0.8
20	0.43	4.2	39	2.4	118	3.1	2.0	2.9
21	1.18	11.6	179	10.8	512	13.5	1.5	2.2
Total (storm events)	4.38	43.2	1425	85.7	3462	91.5	12.7	18.7
Total (year)	10.14	–	1662	–	3784	–	67.8	–

Percentage values were obtained by dividing individual yields by the corresponding annual yields.

Table 5
ANOVA synthesis (F value) for water, sediment and nutrient yields and maximum concentrations during the studied hydrological years.

	Df	Water		Sediment			TP			NO_3^-		
		Yield		Yield	Conc.		Yield	Conc.		Yield	conc.	
Year	2	0.33	ns	0.48	ns	1.77 *	0.81	ns	1.20 *	3.72 **	1.27	*
Season	3	4.93	**	2.26	*	0.81 *s	1.50	*	1.22 *	0.85	ns	0.57 ns

Df, degrees of freedom; ns, non significant; *, **, ***, significant at $P \leq 0.05$, $P \leq 0.01$, and $P \leq 0.001$, respectively.

Minimum load was observed in October, 2011 (event 10), which occurred during a drought period. Storm events were responsible for transferring 60, 6, and 86% of the annual sediment transport in 2010/2011, 2011/2012, and 2012/2013, respectively, despite water yield during these events only amounting to 16, 17, and 43% of each year's annual flow. Sediment transport was shown to be positively correlated at $P < 0.001$ level to FD, W, Pk_n, and Q_{max}; and at $P < 0.01$ level to Q_{mean} and $Q_{peak\ 1}$ (Table 3).

The temporal dynamics in phosphorus transport was similar to suspended sediment. Phosphorus transport during storm events ranged from 4 to 1356 kg. Storm events were responsible for 87, 5, and 92% of the annual phosphorus transport in 2010/2011, 2011/2012, and 2012/2013, respectively. Phosphorus transport also showed dependence on the intensity and amplitude of the storm events as higher loads corresponded generally to larger water yields (Table 3).

Nitrate load also demonstrated large seasonal and annual variability. Nitrate yield was higher mainly during autumns, but also during springs (Fig. 4). However, the differences between seasons are not statistically significant (Tables 5 and 6). The nitrate transported during storm events varied from 0.0×10^3 to 10.2×10^3 kg. The highest nitrate load (10.2×10^3 kg) was registered in October, 2010 (event 2). Storm events were directly responsible for only 20, 17, and 19% of each year's annual load, i.e., the largest portion reached the river during non-storm events. Nitrate was positively correlated at $P < 0.01$ level to the total amount of rainfall registered between the rising and recession limbs of the same storm event (Pe) (Table 3).

From December 19, 2010 to January 9, 2011 it was not possible to measure turbidity directly with the automatic probe due to equipment malfunctioning. Therefore, yield estimates during that time period were obtained from the statistical relationship observed between SSC (or TP) and discharge during the remaining monitored period (Fig. 5). This relationship was represented by a power function as in Langlois et al. (2005) and Lefrançois et al. (2007). The power function suggests that only high discharges lead to large sediment and phosphorus transport. However, it does not include high sediment and phosphorus loads measured in low discharges, i.e., it cannot represent hysteresis events. Therefore, the relationships described in Fig. 5 can eventually lead to some uncertainty when estimating sediment and nutrient yields for the time period (22 days) when the equipment malfunctioned.

3.4. Hysteresis patterns

The relationships between discharge and SSC, TP, PP, SRP, and NO_3^- were analysed for most events observed in the Enxoé catchment. The discharge peaks that were not monitored with sufficient detail, as a result of equipment malfunctioning or insufficient coverage during the rising or recession limbs (soluble elements during the larger storm events) were not analysed for their hysteresis patterns.

Fig. 6 shows a plot of ΔC vs ΔR (Butturini et al., 2006), and summarises C–Q hysteresis loop types of the particulate determinands (SSC, TP, and PP) during the monitored storm event. The components of the particulate matter were located in regions A and D, indicating a flushing behaviour (positive ΔC). Most storm events registered during autumn were located in region A, presenting a clockwise hysteresis loop trajectory (positive ΔR). Events 15 and 16 were the exception, registering anticlockwise loop trajectories in all discharge peaks (region D). Winter and early spring storm events registered mixed (figure-of-eight-shaped hysteresis loops; $\Delta R = 0$) or anticlockwise loop trajectories (negative ΔR). Spring storm events showed contrasting behaviours, with the event observed during the first hydrological year revealing an anticlockwise loop trajectory and the events observed during the third hydrological year presenting clockwise loop trajectories.

Generally, the first peaks of autumn storm events showed larger dispersion of the C–Q hysteresis loops when compared with the remaining events. Those peaks presented a large area ($\Delta R > 20\%$) while all other events had a smaller magnitude ($-20\% < \Delta R < 20\%$). Also, many events (especially those that occurred during early spring) presented a ΔC near 100% indicating that the hysteresis patterns showed a coincidence between the maximum concentration values and maximum discharge, i.e., the delay between concentration and discharge peaks was small.

Fig. 7 shows a plot of ΔC vs ΔR for the soluble elements (SRP, and NO_3^-). SRP was located in all regions of the plot leading to some uncertainty when analysing its hysteresis patterns. Nevertheless, SRP seems to generally have registered a dilution behaviour (negative ΔC) during autumn and a flushing behaviour (positive ΔC) during winter and spring. Most autumn storm events also showed contrasting hysteresis patterns, but during winter, early spring, and spring most hysteresis loops were clockwise ($\Delta R > 0$).

NO_3^- was located in regions B, C, and D in a plot of ΔC vs ΔR. The first storm events registered during autumn presented, in general, a flushing behaviour (positive ΔC) and anticlockwise loop trajectories (negative ΔR). Those C–Q hysteresis loops also revealed a large magnitude ($\Delta R < -20\%$). The remaining storm events showed, in general, a dilution behaviour (negative ΔC) and anticlockwise loop trajectories.

4. Discussion

4.1. Hydrological behaviour

The Enxoé River, as temporary, normally exhibited no flow or ephemeral conditions from June to October (Fig. 2). In the beginning

Table 6
Mean water, sediment and nutrient yields and maximum concentrations during the studied hydrological years.

	Water		Sediment			TP				NO_3^-			
	($\times 10^6$ m^3)		($\times 10^3$ kg)		(mg l^{-1})	(kg)		(mg l^{-1})		($\times 10^3$ kg)		(mg l^{-1})	
Year:													
2010/2011	0.52	a	144.0	a	716.2	b	414.0	a	2.4	ab	4.4	a	12.9	a
2011/2012	0.11	a	1.7	b	214.1	c	4.4	a	1.4	b	1.7	ab	10.3	ab
2012/2013	0.44	a	142.5	a	1364.2	a	346.2	a	4.1	a	1.3	b	9.5	b
Season:														
Autumn	0.23	b	116.2	ab	1315.6	a	345.8	a	4.3	a	2.7	a	12.5	a
Early winter	0.30	b	23.5	b	447.4	b	69.1	b	1.3	b	1.8	a	9.1	a
Early spring	1.01	a	294.6	a	804.1	a	654.0	a	2.4	ab	2.8	a	9.7	a
Spring	0.57	ab	96.8	ab	785.1	ab	282.2	a	2.3	ab	3.7	a	10.6	a

In each year and season, values in the same column followed by the same letter are not significantly different ($P \leq 0.05$).

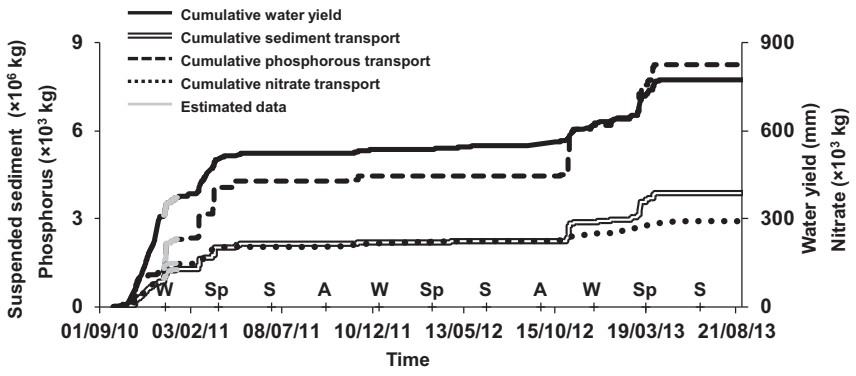

Fig. 4. Cumulative water yield, suspended sediment, total phosphorus, and nitrate yield in the Enxoé catchment between September, 2010 and August, 2013. A, W, Sp, and S indicate the beginning of autumn, winter, spring, and summer, respectively.

of each hydrological year (September/October), the first rain events (events 1, 10, and 12) generated flow peaks followed by a quick recession as the soil was not fully saturated and groundwater flow was greatly diminished. The resulting water yields were quite small, varying between 0.01×10^6 and 0.07×10^6 m^3 (Table 2). From October to December, the soil became increasingly saturated with successive heavy rains. Subsurface flow was enhanced during this period, resulting most times in storm events with multiple discharge peaks (e.g., events 2, 3, and 14). Flow also lasted longer during these events (33 to 127 h). From December to April, the response to rain events still existed as the soil continued to be saturated. Flow duration was dependent on rainfall, lasting from 21 to 234 h. Groundwater flows were also maintained for longer periods, but still tended to fall quickly, especially during months with less rain (January/February). Hence, flow in the Enxoé River was mostly influenced by rainfall events (Table 3), whereas the effect of the groundwater table was minor.

Tables 5 and 6 confirm the strong seasonality of water yield in the Enxoé river. Water yield for storm events occurring during early spring (events 7, 8, 18, and 19) were found to be statistically different when compared to the events registered during winter and autumn. This may be explained by the higher amount of rainfall occurring during that period (Pe varied between 21 and 85 mm) compared with winter events, but also due to the antecedent soil moisture of those events in relation to autumn events; a season which registered a similar rainfall amount (Pe varied from 20 to 84 mm).

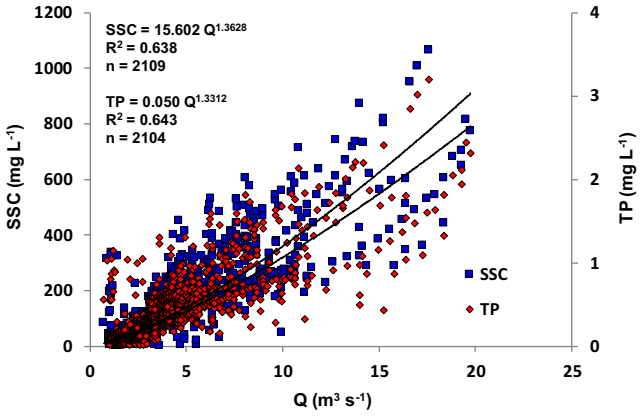

Fig. 5. Relationships of suspended sediment (SSC) and total phosphorus (TP) concentrations versus discharge (Q) in the Enxoé catchment.

4.2. Sediment and nutrient dynamics

4.2.1. Suspended sediments

The strong seasonal and annual variability observed in sediment transport was mostly explained by variations in stream transport capacity and particle availability. Sediment transport was higher during autumn and early spring when the largest storm events took place (Table 5). Sediment was stored at low flow and transported under high discharge conditions, as shown by the high correlation found between sediment transport and W, $Q_{max,}$ Q_{mean}, and $Q_{peak\ 1}$ (Table 3). Tillage operations carried out in agricultural fields were an important mechanism associated with particle availability and sediment transport. During autumn and early spring, tillage operations carried out in Enxoé (Table 1), when heavy rains were also registered (Table 2), ended up enhancing soil erosion by promoting the removal of the soil cover surface provided by crop residues or growing plants, which absorb the energy of raindrops and reduce the erosive energy of runoff during rain events (Kosmas et al., 1997; Nunes et al., 2011).

Another important mechanism associated with sediment transport during autumn was related to bank destruction or trampling caused by cattle pasturing near the river during drier seasons. Bull (1997) estimated that the contribution of bank eroded materials to river sediment systems may vary between less than 5 to over 80%. Pasturing near streams, or even in the river bed, leads to vegetation reduction, affecting flow erosion, bank stability, bank accretion, and bank stabilisation. Bull (1997) also refers to the mechanisms on how vegetation contributes to prevent bank erosion, namely, by retarding the near-bank flow and damping turbulence, by resisting tension and increasing cohesion, and by reducing the impact of moisture and loosening processes, which are a precursor to the removal of materials. Therefore, pasturing the river bed promotes bank erosion, with the ruined bank materials adding to the deposited sediment stock to increase the quantity of available particles that can be easily transported (Lefrançois et al., 2007). In the Enxoé, particle availability was at maximum in the river bed at the beginning of autumn because of pasturing. SSC monitored during the first storm events reached 412 to 3790 mg l^{-1}. Event 12, which took place after the drought of 2011/2012, registered the maximum value observed during the study period. The first storm events were thus responsible for carrying the suspended sediment available in the temporary pools formed along the river or deposited in the river bed to the reservoir (Table 4). These conditions explain the dominant clockwise loop trajectories and the flushing effect registered during the first peak discharge of autumn storms (Table 7; Fig. 6). The following discharge peaks (when multiple flow peaks occurred) were then responsible for carrying sediment from multiple locations (arable lands located upstream), from new deposits originating from a high rate of

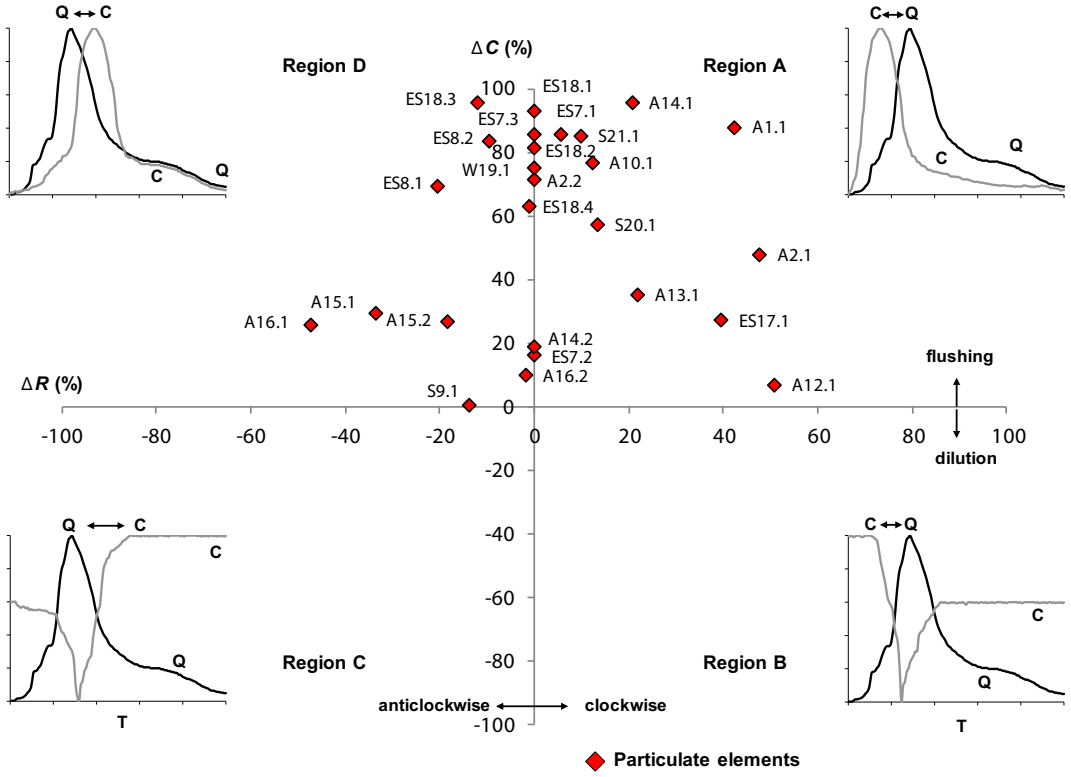

Fig. 6. Plot of ΔC vs ΔR for the C–Q hysteresis loops of particulate elements (SSC, TP, and PP). The marks i,j correspond to the ith storm event monitored (1–21) and the jth discharge peak (1–4) monitored during autumn (A), winter (W), early spring (ES), and spring (S). Illustrations of the typical C–Q relations are presented for each region of the plot ΔC vs ΔR.

bank collapse just after the passage of the first storm peaks (Asselman, 1999), or simply from temporary deposition in the river.

During winter, sediment loads remained generally low (Table 6). Asselman (1999) observed that in a situation where storm events occur in rapid succession (e.g., October/November, 2012), sediment transport becomes progressively reduced because of insufficient time for exhausted sediments to accumulate between events. Sediment transport was predominantly originating from more distant locations, namely soil erosion in agricultural fields, as confirmed by the anticlockwise or mixed patterns registered in the C–Q relation.

During March (early spring), sediment loads increased again (Table 6), as a result of high rainfall rates registered and consequent soil erosion. During these periods, tillage operations were again carried out for sowing spring crops like sunflower, weed control, and fire prevention in the agro-forestry of holm-oaks. These practices again promoted particle availability to runoff (flushing). There was also a return of the cattle to pasturing near the stream with consequent bank erosion. During spring events, sediment transport was again progressively reduced (Table 6). Clockwise and anticlockwise trajectory loops were observed whenever sediments were predominantly transported from the river deposits or from more distant locations upstream, respectively.

Similar sediment transport patterns to those described above for Enxoé have been observed in different regions of the Mediterranean (Rovira and Batalla, 2006; Alexandrov et al., 2007; Nadal-Romero et al., 2008; López-Tarazón et al., 2009; Oeurng et al., 2010a). In Enxoé, 46% of the sediment transport during storm events registered clockwise hysteretic loops, indicating that those sediments had origins predominantly in river bed deposits and nearby source areas, while 43% of the sediment transport registered anticlockwise loop trajectories, revealing a predominance of more distant source areas. The remaining materials arrived at the outlet in a mixed trajectory, thus the source of these sediments was unclear.

Annual sediment yield varied between 13 and 480 kg ha^{-1} y^{-1} (Table 8). The lower value was recorded during a very dry year. Since no major storm events were registered, soil erosion was minimal. The value determined in 2010/2011 (480 kg ha^{-1} y^{-1}) may be viewed as relatively low considering that it was recorded in a humid year. This value is within the same order of magnitude of the values registered for other catchments in the Iberian Peninsula. Rovira and Batalla (2006) estimated a sediment loss of 500 kg ha^{-1} in a catchment located in Cataluña, Spain. In this catchment, more than 90% of the annual sediment load was transported during storm events. Casalí et al. (2010) also reported sediment losses of 550–700 kg ha^{-1} yr^{-1} in two catchments located in Navarre, Spain. Oeurng et al. (2010a) likewise reported sediment losses of 150–700 kg ha^{-1} for a catchment located in the south of France, in which 85–95% of the annual sediment load was transported during storm events. Nonetheless, Walling and Webb (1996) described sediment losses much higher (between 1000 and 2000 kg ha^{-1} yr^{-1}) for other Mediterranean basins of the Iberian Peninsula. The values determined in Enxoé were also within the lowest values of the range reported by de Vente et al. (2006) for Italian basins with similar sizes (4200 to 9100 ha) as the Enxoé catchment.

The Enxoé catchment presents a large area with agro-forestry of holm-oaks and olive groves that play an important role in protecting the soil surface from soil erosion due to the reduced number of tillage operations carried out there. Even the areas with annual crops register agriculture practices that are not very intensive as shown in Table 1 (with fallow being adopted in crop rotations 2 and 3). This explains mostly the relatively low sediment yield losses registered in Enxoé. Rovira and Batalla (2006), Casalí et al. (2010), and Oeurng et al. (2010a) also reported on the contribution of forests and pastures to soil protection. While sediment losses in Enxoé were within the threshold limits (1000–2000 kg ha^{-1} yr^{-1}) suggested by Huber et al. (2008) to be considered as tolerable for the south of Europe, results represent an average value for the entire catchment. Sediment yield was likely higher in areas with arable land than in areas with agro-forestry systems or even olive groves. It is therefore important to adopt prevention measures for reducing soil erosion in those arable areas. Reduced tillage

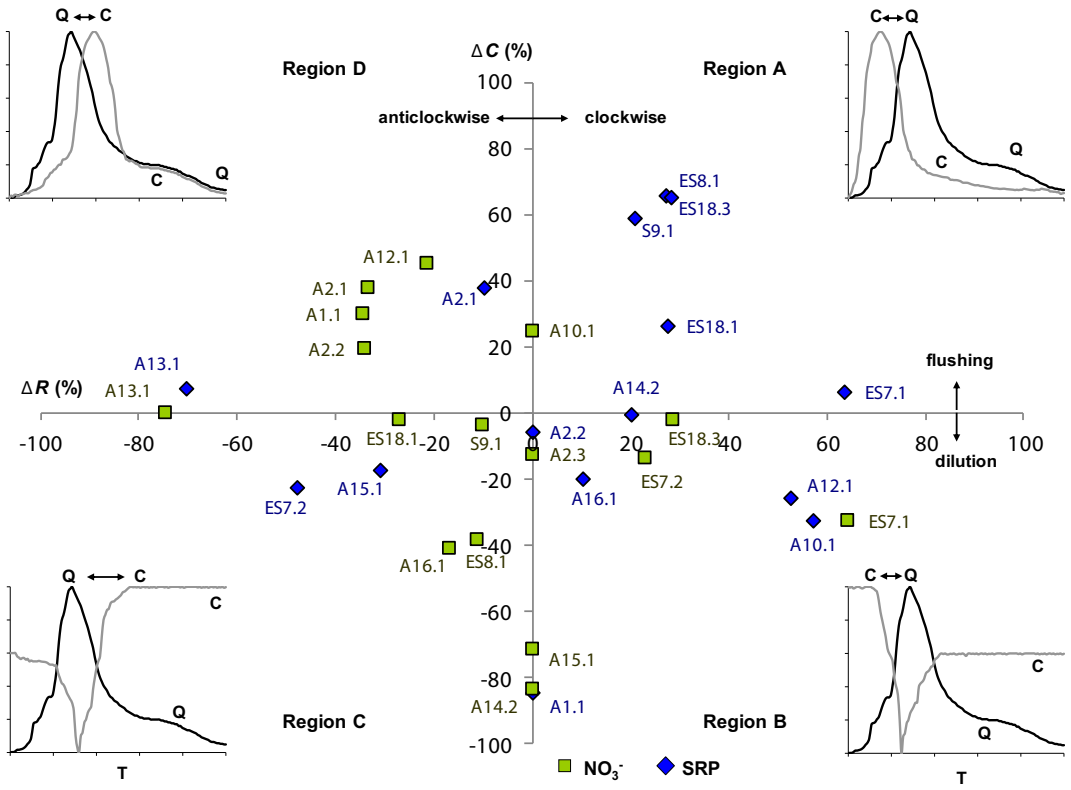

Fig. 7. Plot ΔC vs ΔR for the C–Q hysteresis loops of soluble reactive phosphorus (SRP), and nitrate (NO_3^-). The marks i,j correspond to the ith storm event monitored (1–21) and the jth discharge peak (1–4) monitored during autumn (A), winter (W), early spring (ES), and spring (S). Illustrations of the typical C–Q relations are presented for each region of the plot ΔC vs ΔR.

(or no-till) can be effective in reducing sediment losses by maintaining crop residue on the soil surface and minimising soil particle movement during storms. These techniques are also known to improve water infiltration by promoting soil aggregation which would obviously contribute to reducing runoff. On the other hand, hysteresis patterns showed that there is a large contribution from nearby sources (banks degradation, temporary deposits, etc.) to sediment loads during storm events. Therefore, protecting the river banks from pasturing may also help improving bank stability and cohesion, thus minimising sediment transport.

4.2.2. Phosphorus forms

Total and particulate phosphorus dynamics revealed the same hysteresis patterns as observed for sediment transport since they were obtained from turbidity measurements (Eq. (6) and (7)). Thus, the same clockwise and anticlockwise flushing effects referred to earlier for SSC were also observed here (Table 7). SRP hysteresis patterns during autumn varied considerably between events. Although most autumn events produced clockwise trajectories during the first peak discharge, there is no clear identification of SRP origins during that period. During spring, P may also have been supplied to annual summer crops (Table 1), but the clockwise trajectories observed during early spring and spring storms seem to be mostly explained by the return of the cattle pasturing near the stream and eventual increase of SRP concentration in the river (Table 7).

Annual phosphorus losses varied between 0.04 and 0.96 kg ha^{-1} y^{-1} during the monitored period (0.3–6.5% of P inputs; Table 8). The lower value occurred when no major storm events were registered (2011/2012). P loads observed in 2010/2011 and 2012/2013 can be considered relatively high when compared with reported P losses. Casalí et al. (2010) presented similar high values (0.76 kg P ha^{-1} yr^{-1})) in one of the catchments studied in Navarra (Spain), but found lower P exports (0.35 kg P ha^{-1} yr^{-1}) in the other catchment studied in the same region. Tzoraki and Nikolaidis (2007) only found loads of 0.10 kg P ha^{-1} (1.2% of input) in a mountain forested catchment in Greece. Probst (1985) reported equally low exportation rates (1%) for his case study. Klein and Koelmans (2011) reported data on P exports (0.08–0.88 kg P ha^{-1} yr^{-1}) for 13 central European basins, in which the Enxoé values (mean = 0.61 kg ha^{-1} y^{-1}) would be slightly higher than the average. Nonetheless, all these values are much lower than the 1.2–1.7 kg P ha^{-1} yr^{-1} loads reported in the UK by Brazier et al. (2005).

Phosphorus loads to the Enxoé reservoir were thus relatively high during the wet year, which may partially explain the frequent toxic algae bloom observed in the reservoir since its construction. However, the largest part arrived at the reservoir in the particulate form and was therefore deposited at the bottom, being only available to algae after mineralisation of phosphorus organic forms. Furthermore, despite in most events SRP constituted only a small fraction of TP, the 6 events where the fraction of SRP/TP was higher than 35% may have had a more negative contribution to the eutrophication of the Enxoé reservoir than all the remaining events since SRP is directly absorbed by algae. The same practices (reduced tillage and river bank protection) recommended earlier for controlling soil erosion should also be adopted for reducing P loads to the reservoir.

4.2.3. Nitrate

Rainfall (as explained by the significant correlation found in Table 3 between nitrate transport and Pe) and soil hydraulic characteristics were the main characteristics influencing nitrate transport in Enxoé. Land management, namely crop fertilisation periods, influenced nitrate availability.

Nitrate losses were mostly observed during autumn and early spring (Table 2). However, differences between seasons were not significantly different (Table 6). Nonetheless, those two seasons registered the most important rainfall events and corresponded to crop fertilisation periods. During autumn, fertilisation was applied to annual winter crops during

Table 7
Conceptual model of the source and transport of sediments and nutrients in the river Enxoé catchment area.

	Autumn			Winter			Early spring/spring			Summer		
	Source	Transfer	Pattern	Source	Transfer	Pattern	Source	Transfer	Pattern	Source	Transfer	Pattern
Particulate elements												
– SSC, TP, and PP	River banks	Runoff	Flushing Clockwise	Agricultural fields	Runoff	Flushing Mixed	River banks Agricultural fields	Runoff	Flushing Mixed	No flow	–	–
Soluble elements												
– SRP	River banks Agricultural fields	Runoff lateral flow	Dilution Mixed	River banks	Runoff	Flushing Clockwise	River banks	Runoff	Flushing Clockwise	No flow	–	–
– NO_3^-	Agricultural fields	Lateral flow	Flushing Anticlockwise	Agricultural fields	Lateral flow	Dilution Mixed	Agricultural fields	Lateral flow	Dilution Anticlockwise	No flow	–	–

SSC, suspended sediment concentration, TP, total phosphorus, PP, particulate phosphorus, SRP, soluble reactive phosphorus, NO_3^-, nitrate.

sowing, which normally involved burying fertilisers, thus preventing N losses by runoff. During late-winter/spring, fertilisation was applied to summer crops also during sowing. Additionally, annual winter crops were fertilised to promote tilling (February/March) and increased crop yield. However, fertilisers here were usually applied to the soil surface, increasing the odds of N losses by runoff (e.g., event 7) as well as leaching with rainfall.

Hysteresis patterns observed during the monitored events showed predominantly anticlockwise trajectories. NO_3^- infiltrated first in the soil only reaching later the water stream through subsurface flow. Nitrate transport was thus dependent on the soil physical and hydraulic characteristics, i.e., soil texture, soil porosity, soil water retention, and soil hydraulic conductivity, which influenced subsurface flow and the delay in the concentration–discharge peak. Buda and DeWalle (2009), Oeurng et al. (2010b), Zhu et al. (2012) noted similar preferential flowpaths with nitrate losses being associated with either subsurface flow or baseflow.

Hence, peak discharges were not directly associated with nitrate transport, with only 17–20% of the annual yield being monitored during storm events (Table 4). The flushing effect and the anticlockwise loops observed during autumn (Fig. 7) showed that large amounts of nitrate were transported predominantly from distant areas of the catchment in the days after those storm events, namely from the agricultural fields where fertilisation occurred. This flushing mechanism was explained by the successive rainfall events registered during that period, soil moisture close to saturation, and the medium to coarse textures of the relatively shallow soils in the catchment, namely Luvisols and Cambisols which represent 78% of the area (Ocampo et al., 2006). The available soil information in this region shows saturated hydraulic conductivity (K_s) values varying between 129 and 549 cm d^{-1}, and total porosity (φ) values ranging from 0.40 to 0.51 (Ramos et al., 2013). These characteristics favoured subsurface water flow in most part of the area, leaching large amounts of nitrate applied to annual winter crops during sowing.

During winter and early spring/spring the flushing mechanism switched to a dilution behaviour (Table 7). Nitrate concentrations in the river always decreased with the arrival of the discharge peak, i.e., the arrival of "clean" water from non-fertilised areas, such as agroforestry of holm-oaks and permanent pastures, which partially diluted river flow. Hence, there was no nitrate being transported across the catchment with the exception of that due to the soil leaching originating in the annual winter crop areas.

Nitrogen applied either from fertilisation or livestock under different N forms amounted to 51 kg N ha^{-1} y^{-1} (Table 1). Besides nutrient uptake, various N transformation processes then occurred in soils mostly due to microbial activity, which was controlled by soil environmental conditions, such as soil water and temperature (Lillebø et al., 2007). From the initial inputs, between 1.0 and 10.3 kg N ha^{-1} y^{-1} arrived at the reservoir in the nitrate form, i.e., between 4.4 and 45.5 kg NO_3^- ha^{-1} y^{-1}. Nitrate exports in Enxoé can thus be considered low, which is justified by the fact that agriculture and pasturing in the region are extensive. Nitrate yields fall within the same order of magnitude as those found by Oeurng et al. (2010b) and Probst (1985) for catchments in the south of France. There, nitrate loads varied from 10 to 50 kg NO_3^- ha^{-1}. Casalí et al. (2010) also reported values ranging from 22 to 54 kg NO_3^- ha^{-1} in the two catchments studied in Navarre (Spain). In terms of N units, Tzoraki and Nikolaidis (2007) reported losses of 2.73 kg N ha^{-1} (11% of input) in their case study (forested areas were here the dominant land use with 75.4% of the area). But, compared with the values of Klein and Koelmans (2011) for catchments in Central Europe (0.8–42.6 kg N ha^{-1} yr^{-1}), N exports in the Enxoé catchment are within the lowest values.

The identification of nitrate sources in the Enxoé catchment using hysteresis patterns was relatively clear due to the small size of the catchment and predominant land uses and land management. Nitrate losses were associated with non-point sources but the periods when higher exports were observed always corresponded to fertilisation periods of annual winter and summer crops. Nitrate losses were relatively low though but could be further minimised by reducing applications at the tilling crop stages during rainy years or by preserving riparian vegetation which would partially use some of the nitrate exported to the river before it reached the reservoir.

Table 8
Annual water, sediment, and nutrient yields in the Enxoé catchment between September, 2010 and August, 2013.

Year	Water yield		Sediment		P		N	
	(mm)	(%)	(kg ha^{-1})	(%)	(kg ha^{-1})	(%)	(kg ha^{-1})	(%)
2010/2011	523	69.3	480	–	0.96	6.5	10.3	20.1
2011/2012	28	8.5	13	–	0.04	0.3	1.0	1.9
2012/2013	225	35.7	369	–	0.84	5.7	3.4	6.7

Percentage values were obtained by dividing annual yields by catchment inputs.

5. Conclusions

This study summarises findings after three years of intense hydro-biogeochemical monitoring in the Enxoé temporary river, located in a Mediterranean region, and draining an agricultural catchment. Sediment and phosphorous dynamics in the Enxoé catchment are associated with the stream transport capacity and particle availability. Sediment and phosphorus dynamics showed a strong seasonal and annual variability during the monitored period. Differences were found to be statistically significant between years and seasons, with high sediment and phosphorus concentration values and large yields occurring during autumn and early spring events. These were related with tillage operations and cattle pasturing, which promoted the increase of solid transport during autumnal and early spring episodes.

The first storm events after summer registered the highest monitored concentrations, as the particulate matter deposited in the river bed was transported to the reservoir with early rains. However, water yield in those events was relatively small (0.01×10^6 and 0.07×10^6 m^3) since soils were still dry, and thus sediment and phosphorus yields were also low. Nevertheless, storm events were responsible for transferring the major amount (60–92%) of sediment and phosphorus to the reservoir.

The behaviour of the soluble elements was in general different from the particulate ones. SRP patterns were relatively confusing. Thus, a larger number of events need to be monitored in order to identify the "most probable SRP-Q response" for Enxoé. Autumn and early spring events registered also the highest nitrate exports. However, the contribution of storm events to NO_3^- loads was minor (17–20% of the annual losses). The largest portion was transported from agricultural fields during non-storm events, through subsurface flow.

Acknowledgements

This research was performed within the framework of the EU Interreg SUDOE IVB programme (SOE1/P2/F146 AguaFlash project, http://www.aguaflash-sudoe.eu), and the Project EUTROPHOS (PTDC/AGR-AAM/098100/2008) of the Fundação para a Ciência e a Tecnologia (FCT).

References

Agroscope, 2009. Données de base pour la fumure des grandes cultures et des harbages. Rev. Suisse d'Agric. 41 (1).
C.C.D.R. Alentejo, 2005. Anuário de recursos hídricos do Alentejo. Ano Hidrológico 2003/2004. MAOTDR, Évora, Portugal.
Alexandrov, Y., Laronne, J.B., Reid, I., 2003. Suspended sediment concentration and its variation with water discharge in a dryland ephemeral channel, northern Negev, Israel. J. Arid Environ. 53, 73–84.
Alexandrov, Y., Laronne, J.B., Reid, I., 2007. Intra-event and inter-seasonal behaviour of suspended sediment in flash floods of the semi-arid northern Negev, Israel. Geomorphology 85, 85–97. http://dx.doi.org/10.1016/j.geomorph.2006.03.013.
APHA, 1995. Standard Methods. 19th edition. American Public Health Association, Washington, DC.
Asselman, N.E.M., 1999. Suspended sediment dynamics in a large drainage basin: the River Rhine. Hydrol. Process. 13, 1437–1450.
Borrelli, P., Märker, M., Panagos, P., Schütt, 2014. Modeling soil erosion and river sediment yield for an intermountain drainage basin of the Central Apennines, Italy. Catena 114, 45–58.
Bowes, M.J., House, W.A., Hodgkinson, R.A., Leach, D.V., 2005. Phosphorus-discharge hysteresis during storm events along a river catchment: the River Swale, U.K. Water Res. 39, 751–762.
Brazier, R.E., Heathwaite, A.L., Liu, S., 2005. Scaling issues relating to phosphorus transfer from land to water in agricultural catchments. J. Hydrol. 304, 330–342.
Buda, A.R., DeWalle, D.R., 2009. Dynamics of stream nitrate sources and flow pathways during stormflows on urban, forest and agricultural watersheds in central Pennsylvania, USA. Hydrol. Process. 23, 3292–3305.
Bull, L.J., 1997. Magnitude and variation in the contribution of bank erosion to the suspended sediment load of the river Severn, UK. Earth Surf. Process. Landf. 22, 1109–1123.
Burt, T.P., 2003. Monitoring change in hydrological systems. Sci. Total Environ. 310, 9–16.
Butturini, A., Gallart, F., Latron, J., Vazquez, E., Sabater, F., 2006. Cross-site comparison of variability of DOC and nitrate C–Q hysteresis during the autumn–winter period in three Mediterranean headwater streams: a synthetic approach. Biogeochemistry 77, 327–349.
Butturini, A., Alvarez, M., Bernal, S., Vazquez, E., Sabater, F., 2008. Diversity and temporal sequences of forms of DOC and NO_3-discharge responses in an intermittent stream: predictable or random succession? J. Geophys. Res. 113, G03016. http://dx.doi.org/10.1029/2008JG000721.
Casalí, J., Giménez, R., Díez, J., Álvarez-Mozos, J., Valle, Del, de Lersundi, J., Goñi, M., Campo, M.A., Chahor, Y., Gastesi, R., López, J., 2010. Sediment production and water quality of watersheds with contrasting land use in Navarre (Spain). Agric. Water Manage. 97, 1683–1694.
Cerro, I., Sánchez-Pérez, J.M., Ruiz-Romera, E., Antigüedad, I., 2013. Variability of particulate (SS; POC) and dissolved (DOC, NO_3) matter during storm events in the Alegria agricultural watershed. Hydrol. Process. http://dx.doi.org/10.1002/hyp.9850.
de Vente, J., Poesen, J., Bazzoffi, P., van Rompaey, A., Verstraeten, G., 2006. Predicting catchment sediment yield in Mediterranean environments: the importance of sediment sources and connectivity in Italian drainage basins. Earth Surf. Process. Landf. 31, 1017–1034.
Eder, A., Strauss, P., Krueger, T., Quinton, J.N., 2010. Comparative calculation of suspended sediment loads with respect to hysteresis effects (in the Petzenkirchen catchment, Austria). J. Hydrol. 389, 168–176.
Hendrilsen, A., Selmer-Olsen, A.R., 1970. Automatic methods for determination of nitrate and nitrite in water and soil extracts. Analyst 95, 514–518.
House, W.A., Warwick, M.S., 1998. Hysteresis of the solute concentration/discharge relationship in rivers during storms. Water Res. 32, 2279–2290.
Huber, S., Prokop, G., Arrouays, D., Banko, G., Bispo, A., Jones, R.J.A., Kibblewhite, M.G., Lexer, W., Möller, A., Rickson, R.J., Shishkov, T., Stephens, M., Toth, G., Van den Akker, J.J.H., Varallyay, G., Verheijen, F.G.A., Jones, A.R. (Eds.), 2008. Environmental Assessment of Soil for Monitoring: Volume I Indicators & Criteria. EUR 23490 EN/1. Office for the Official Publications of the European Communities, Luxembourg (339 pp.).
Instituto da Água, 2008. Poluição provocada por nitratos de origem agrícola. Directiva 91/676/CEE, de 12 de Dezembro de 1991. Relatório (2004–2007). Publicação conjunta do MAOTDR e MADRP, Lisboa, Portugal.
Klein, J.J.M., Koelmans, A.A., 2011. Quantifying seasonal export and retention of nutrients in West European lowland rivers at catchment scale. Hydrol. Process. 25, 2102–2111.
Kosmas, C., Danalatos, N., Cammeraat, L.H., Chabart, M., Diamantopoulos, J., Farand, R., Gutierrez, L., Jacob, A., Marques, H., Martinez-Fernandez, J., Mizara, A., Moustakas, N., Nicolau, J.M., Oliveros, C., Pinna, G., Puddu, R., Puidefabregas, J., Roxo, M., Simao, A., Stamou, G., Tomasi, N., Usai, D., Vacca, A., 1997. The effect of land use on runoff and soil erosion rates under Mediterranean conditions. Catena 29, 45–59.
Langlois, J.L., Johnson, D.W., Mehuys, G.R., 2005. Suspended sediment dynamics associated with snowmelt runoff in a small mountain stream of Lake Tahoe (Nevada). Hydrol. Process. 19, 3569–3580.
Lefrançois, J., Grimaldi, C., Gascuel-Odoux, C., Gilliet, N., 2007. Suspended sediment and discharge relationships to identify bank degradation as a main sediment source on small agricultural catchments. Hydrol. Process. 21, 2923–2933.
Lillebø, A.I., Morais, M., Guilherme, P., Fonseca, R., Serafim, A., Neves, R., 2007. Nutrient dynamics in Mediterranean temporary streams: a case study in Pardiela catchment (Degebe River, Portugal). Limnologica 37, 337–348.
López-Tarazón, J.A., Batalla, R.J., Vericat, D., Francke, T., 2009. Suspended sediment transport in a highly erodible catchment: the River Isábena (Southern Pyrenees). Geomorphology 109, 210–221.
MADRP, 2010. Análise dos impactos no solo resultantes da introdução de novos olivais regados no Alentejo. 2° Relatório do Grupo de Trabalho do Olival. INRB, MADRP, Lisboa.
Martínez-Carreras, N., Krein, A., Udelhoven, T., Gallart, F., Iffly, J.F., Hoffman, L., Pfister, L., Walling, D.E., 2010. A rapid spectral-reflectance-based fingerprinting approach for documenting suspended sediment sources during storm runoff events. J. Soils Sediments 10, 400–413.
Motha, J.A., Wallbrink, P.J., Hairsine, P.B., Grayson, R.B., 2003. Determining the source of suspended sediment in a forested catchment in southeastern Australia. Water Resour. Res. 39, 1056. http://dx.doi.org/10.1029/2001WR000794.
Nadal-Romero, E., Regues, D., Latron, J., 2008. Relationships among rainfall, runoff, and suspended sediment in a small catchment with badlands. Catena 74, 127–136.
Nunes, A.N., Almeida, A.C., Coelho, C.O.A., 2011. Impacts of land use and cover type on runoff and soil erosion in a marginal area of Portugal. Appl. Geogr. 31, 687–699.
Ocampo, C.J., Oldham, C.E., Sivapalan, M., Turner, J.V., 2006. Hydrological versus biogheochemical controls on catchment nitrate export: a test of the flushing mechanism. Hydrol. Process. 20, 4269–4286.
Oeurng, C., Sauvage, S., Sánchez-Pérez, J.M., 2010a. Dynamics of suspended sediment transport and yield in a large agricultural catchment, southwest France. Earth Surf. Proc. Landf. 35, 1289–1301.
Oeurng, C., Sauvage, S., Sánchez-Pérez, J.M., 2010b. Temporal variability of nitrate transport through hydrological response during flood events within a large agricultural catchment in south-west France. Sci. Total Environ. 409, 140–149.
Oeurng, C., Sauvage, S., Sanchez-Pérez, J.M., 2011. Assessment of hydrology, sediment and particulate organic carbon yield in a large agricultural catchment using the SWAT model. J. Hydrol. 401, 145–153.
Probst, J.L., 1985. Nitrogen and phosphorus exportation in the Garonne Basin (France). J. Hydrol. 76, 281–305.
Ramos, T.B., Gonçalves, M.C., Brito, D., Martins, J.C., Pereira, L.S., 2013. Development of class pedotransfer functions for integrating water retention properties into Portuguese soil maps. Soil Res. 51, 262–277.
Rovira, A., Batalla, R.J., 2006. Temporal distribution of suspended sediment transport in a Mediterranean basin: the Lower Tordera (NE Spain). Geomorphology 79, 58–71.
Sánchez-Pérez, J.M., Vervier, P., Garabétian, F., Sauvage, S., Loubet, M., Rols, J.L., Bariac, T., Weng, P., 2003. Nitrogen dynamics in the shallow groundwater of a riparian wetland zone of the Garonne, SW France: nitrate inputs, bacterial densities, organic matter supply and denitrification measurements. Hydrol. Earth Syst. Sci. 7, 97–107.
Siebert, C., Rödiger, T., Mallast, U., Gräbe, A., Guttman, J., Laronne, J.B., Storz-Peretz, Y., Greenman, A., Salameh, E., Al-Raggad, M., Vachtman, D., Zvi, A.B., Ionescu, D., Brenner, A., Merz, R., Geyer, S., 2014. Challenges to estimate surface- and groundwater flow in arid region: the Dead Sea catchment. Sci. Total Environ. 485–486, 828–841.
Skoulikidis, N., Amaxidis, Y., 2009. Origin and dynamics of dissolved and particulate nutrients in a minimally disturbed Mediterranean river with intermittent flow. J. Hydrol. 373, 218–229.
Stevens, C.J., Quinton, J.N., 2008. Investigating source areas of eroded sediments transported in concentrated overland flow using rare earth element tracers. Catena 74, 31–36.
Torrent, J., Barberis, E., Gil-Sotres, F., 2007. Agriculture as a source of phosphorus for eutrophication in southern Europe. Soil Use Manage. 23, 25–35.
Tzoraki, O., Nikolaidis, N.P., 2007. A generalized framework for modeling the hydrologic and biochemical response of a Mediterranean temporary river basin. J. Hydrol. 346, 112–121.
Wallbrink, P.J., Martin, C.E., Wilson, C.J., 2003. Quantifying the contributions of sediment, sediment-P and fertilizer-P from forested, cultivated and pasture areas at the landuse

and catchment scale using fallout radionuclides and geochemistry. Soil Till. Res. 69, 53–68.
Walling, D.A., 2005. Tracing suspended sediment sources in catchments and river systems. Sci. Total Environ. 344, 159–184.
Walling, D.A., Webb, B.W., 1996. Erosion and Sediment Yield: A Global Overview. IAHS Publications 236. IAHS Press, Wallingford, pp. 3–19.
Yevenes, M.A., Mannaerts, C.M., 2011. Seasonal and land use impacts on the nitrate budget and export of a mesoscale catchment in Southern Portugal. Agric. Water Manage. 102, 54–65.
Zhu, Q., Schmidt, J.P., Bryant, R.B., 2012. Hot moments and hot spots of nutrient losses from a mixed land use watershed. J. Hydrol. 414–415, 393–404.